Published in final edited form as:
J Med Chem. 2013 February 14; 56(3): 1276–1290. doi:10.1021/jm3017305.

Potent Elastase Inhibitors from Cyanobacteria: Structural Basis and Mechanisms Mediating Cytoprotective and Anti-inflammatory Effects in Bronchial Epithelial Cells

Lilibeth A. Salvador[†], **Kanchan Taori**[†], **Jason S. Biggs**[‡], **Jean Jakoncic**[§], **David A. Ostrov**[⊥], **Valerie J. Paul**[||], and **Hendrik Luesch**[*,†]

[†]Department of Medicinal Chemistry, University of Florida, Gainesville, Florida 32610, USA

[‡]University of Guam Marine Laboratory, Mangilao, Guam 96923, USA

[§]Brookhaven National Laboratory, Upton, New York 11973, USA

[⊥]Department of Pathology, Immunology and Laboratory Medicine, University of Florida Gainesville, Florida 32610, USA

[||]Smithsonian Marine Station, Fort Pierce, Florida 34949, USA

Abstract

We discovered new structural diversity to a prevalent, yet medicinally underappreciated, cyanobacterial protease inhibitor scaffold and undertook comprehensive protease profiling to reveal potent and selective elastase inhibition. SAR and X-ray cocrystal structure analysis allowed a detailed assessment of critical and tunable structural elements. To realize the therapeutic potential of these cyclodepsipeptides, we probed the cellular effects of a novel and representative family member, symplostatin 5 (**1**), which attenuated the downstream cellular effects of elastase in an epithelial lung airway model system, alleviating clinical hallmarks of chronic pulmonary diseases such as cell death, cell detachment and inflammation. This compound attenuated the effects of elastase on receptor activation, proteolytic processing of the adhesion protein ICAM-1, NF-κB activation and transcriptomic changes, including the expression of pro-inflammatory cytokines *IL1A*, *IL1B* and *IL8*. Compound **1** exhibited activity comparable to the clinically-approved elastase inhibitor sivelestat in short-term assays and demonstrated superior sustained activity in longer-term assays.

Introduction

Cyanobacteria, whether of marine, terrestrial or freshwater origin, have consistently yielded serine protease inhibitors characterized by a conserved 19-membered cyclic hexadepsipeptide core bearing the modified glutamic acid residue 3-amino-6-hydroxy-2-piperidone (Ahp) and a highly variable pendant side chain.[1–3] The isolation of over 100 members of this group of cyanobacterial metabolites, together with antiproteolytic activity data primarily against the serine proteases elastase, chymotrypsin, and trypsin, has provided insights into the importance of the Ahp moiety and the adjacent residue on its N-terminal

Corresponding Author: H.L.: phone, +1-352-273-7738; fax, +1-352-273-7741; luesch@cop.ufl.edu.
H. Luesch is co-founder of Oceanyx Pharmaceuticals, Inc., which is negotiating licenses for patent applications related to the subject matter.

Supporting Information. Supporting information includes details on the structure elucidation of compound **2**–**6**, enantioselective analysis for **1**–**6**, seven tables, five figures, and 1D and 2D NMR spectra of **1**–**6.** This material is available free of charge via the Internet at http://pubs.acs.org.

side which confer selectivity.[1,4] The role of these moieties was elegantly demonstrated through X-ray cocrystallization of A90720A–trypsin and scyptolin–elastase complexes.[5,6] Not found in terrestrial or freshwater cyanobacteria is the 2-amino-2-butenoic acid (Abu) moiety, which is hypothesized to contribute to higher potency.[7] The majority of the marine-derived cyanobacterial metabolites in this class bear the Abu moiety adjacent to the Ahp residue. These compounds, which include lyngbyastatins 4–10, showed potent antiproteolytic activity against elastase with low nanomolar IC_{50}s, and are perhaps among the most potent small molecule inhibitors of elastase.[7–9] Therefore, these small molecules are attractive therapeutics for elastase-mediated pathologies, as well as molecular probes to elucidate critical interactions for effective enzyme inhibition and to interrogate specific intracellular and extracellular molecular targets of elastase. However, limited SAR and a lack of information beyond enzymatic assay data hinder further development of these compounds as small molecule therapeutics.

Elastase is a broad-spectrum enzyme that preferentially cleaves on the C-terminus of small hydrophobic amino acids such as Gly, Ala, and Val and degrades collagen, elastin, fibronectin and components of the extracellular matrix.[10] Elastase has been linked to several diseases involving chronic inflammatory conditions such as chronic obstructive pulmonary disease (COPD), asthma, cystic fibrosis, and systemic inflammatory response syndrome, where there is a protease–antiprotease imbalance.[10,11] Current therapies for these diseases are aimed at alleviating the symptoms but not disease progression, which may be related to the role of elastase.[12] Sivelestat is the only approved drug targeting elastase;[13] however, clinical approval in the United States and Europe has been stalled due to marginal clinical effects.[14] Finding new small molecule therapeutics for COPD is of importance since the disease has been recognized as a major public health problem and the fourth leading cause of death worldwide.[15] Intratracheal instillation of elastase in animal models showed changes such as enlargement of alveolar space, thickening of alveolar septae and mucus hypersecretion, comparable to clinical observations.[16] This enzyme has also been implicated in cell death, transcriptional and translational modulation and processing of pro-inflammatory cytokines, chemokines and adhesion molecules, which also dictate downstream cellular effects.[11] Development of elastase inhibitors has been particularly challenging because of overlapping functions of elastase with those of other serine proteases, as well as limited information on the role of elastase in the progression of disease. Here we comprehensively characterized new elastase inhibitors from marine cyanobacteria and defined superior cellular effects compared with sivelestat.

Results

Isolation and Structure Elucidation

The lyophilized red cyanobacterium collected from Cetti Bay, Guam was extracted with EtOAc–MeOH (1:1) to afford the nonpolar extract. Liquid-liquid partitioning of the nonpolar extract yielded the hexanes-, *n*-BuOH- and H_2O-soluble fractions. The ^{1}H NMR spectrum of the *n*-BuOH fraction showed characteristic resonances for peptides and modified peptides. This fraction was further purified by silica column chromatography and reversed-phase HPLC to give six new Ahp-containing cyclic depsipeptides, termed symplostatins 5–10 (**1**–**6**)(Figure 1).

The major compound, symplostatin 5 (**1**) (Figure 1), showed a pseudomolecular ion of 1044.3981 $[M + Na]^+$, suggesting a molecular formula of $C_{47}H_{64}N_7O_{15}SNa$. LRESIMS using negative ionization showed a loss of 46 amu (*m/z* 998.5 $[M – Na]^–$) relative to the pseudomolecular $[M + Na]^+$ ion. This corresponds to loss of 2 × Na^+ ions and supported that **1** was present as a sodium salt. The ^{1}H NMR spectrum of **1** showed characteristic signals for peptides and modified peptides such as secondary amide protons (δ_H 8.18, 7.71, 7.40, 7.34),

N-CH_3 protons (δ_H 2.77), and α-protons for amino acids (δ_H 3.80–5.10). Analysis of the COSY, TOCSY, HSQC and HMBC data acquired in DMSO-d_6 established the presence of Val, Thr, Ile, *N*-Me-Phe, Phe and the modified amino acids Ahp and Abu (Table 1). Among the three remaining spin systems, one is a distinctive methine quartet (δ_H 6.50) that showed a COSY correlation to a CH_3 doublet (δ_H 1.47) (Table 1). HMBC correlations of the latter to a carbonyl at δ_C 162.9 and a quaternary sp^2 C (δ_C 130.0), together with a TOCSY correlation to a broad NH singlet (δ_H 9.24), established this unit as Abu. The observed low-field methine signal at δ_C/δ_H 73.4/5.03 together with a hydroxy proton resonating at δ_H 6.05 in **1** are distinctive for the Ahp unit. The presence of this cyclized amino acid residue was further supported by COSY and HMBC correlations (Table 1). The remaining spin systems consisted of a low-field methine (δ_C/δ_H 79.9/3.98), an oxygenated diastereotopic methylene (δ_C/δ_H 66.1/3.90, 3.73) and an $-OCH_3$ group (δ_C/δ_H57.1/3.33). From COSY and HMBC analysis, this moiety corresponds to a modified glyceric acid, where the C-2 and C-3 positions are methoxylated and sulfated, respectively (Table 1). The linear sequence of 2-*O*-CH_3 glyceric acid sulfate–Val–Thr–Abu–Ahp–*N*-Me-Phe–Phe–Ile was established using HMBC and NOESY correlations. In order to fulfill the molecular formula requirements and to account for the low-field ^1H NMR chemical shift of the vicinal methine of Thr (δ_H 5.52), additional anisotropic effect from a carbonyl group must be present, and this indicated cyclization of **1** via the carbonyl group of Ile and the hydroxy group of Thr.

The structures of compounds **2**–**6** (Figure 1) were also elucidated using 1D and 2D NMR data and comparison of ^1H and ^{13}C NMR chemical shifts with that of **1** (Supporting Information). Absolute configurations of the stereocenters in **1**–**6** were assigned by enantioselective HPLC-MS analysis of acid hydrolysates with and without prior oxidation of the Ahp unit (Supporting Information).

Enzyme Inhibition

We tested the antiproteolytic activity of **1**–**6** against porcine pancreatic elastase. Compounds **1**–**6** potently inhibited porcine pancreatic elastase with IC_{50}s of 37–89 nM (Table 2), which was comparable to the activity of the related compounds lyngbyastatins 4 and 7. Compounds **4**–**6**, containing N-Me-Tyr, are slightly more potent than their *N*-Me-Phe congeners (**1**–**3**) in inhibiting elastase. In contrast, Ile to Val substitution in the macrocycle and pendant side chain did not affect activity. To demonstrate that these compounds also inhibit the disease-relevant human neutrophil elastase, we determined the antiproteolytic activity against this enzyme. Compounds **4**–**6** and lyngbyastatins 4 and 7 potently inhibited human neutrophil elastase, while symplostatins 5–7 (**1**–**3**) gave higher IC_{50}s (Table 2). Compounds **4**–**6** and lyngbyastatins 4 and 7 showed higher potency than the drug sivelestat, a selective human neutrophil elastase inhibitor, while **1**–**3** had similar activity as sivelestat. Compounds **1**–**6** and lyngbyastatins 4 and 7 were analogously tested for antiproteolytic activity against human and bovine pancreatic chymotrypsin. All the compounds tested were less potent inhibitors of chymotrypsin than elastase (Table 2).

To determine the selectivity of the cyanobacterial elastase inhibitors, we screened the most potent inhibitor lyngbyastatin 7 at a single concentration against a panel of 68 proteases (Figure 2A). Lyngbyastatin 7 showed preferential inhibition for serine proteases at 10 μM, completely inhibiting the serine proteases elastase, chymotrypsin and proteinase K. The serine proteases cathepsin G, kallikrein 8, kallikrein 12 and plasma kallikrein, the dipeptidyl peptidase cathepsin C and the cysteine proteases caspases 1, 9 and 11 were partially inhibited. Lyngbyastatin 7 did not inhibit any member of the cysteine carboxypeptidases, metalloproteases or aspartic family of proteases. To validate the serine protease selectivity profile for this class of inhibitors, a dose-response study against the same panel of 26 serine proteases was undertaken for the most abundant compound, **1** (Figure 2B). Compound **1**,

like lyngbyastatin 7, preferentially inhibited elastase over chymotrypsin. Aside from these enzymes, the majority of the serine proteases including proteinase K was less potently inhibited by **1** than by lyngbyastatin 7, with IC_{50}s of 10 μM or higher.

Molecular Basis for Elastase Inhibition by Lyngbyastatins and Symplostatins

In order to understand the potent and selective inhibitory activity of the Abu-bearing cyclic depsipeptides against elastase, we cocrystallized the most potent inhibitor, lyngbyastatin 7, with porcine pancreatic elastase using the hanging drop vapor diffusion method. The structure of the lyngbyastatin 7–porcine pancreatic elastase complex was solved at a resolution of 1.55 Å, the best reported for an elastase–cyclic depsipeptide inhibitor complex. The elastase complexes with the natural products scyptolin (no Abu) and FR901277 (bicyclic) were previously cocrystallized and analyzed at resolutions of 2.8 Å and 1.6 Å, respectively.[6,17] Porcine pancreatic elastase, despite sharing only 40% amino acid sequence homology to human neutrophil elastase, is an accepted model system to understand key enzyme–inhibitor interactions.[18] They are structurally comparable and share analogous residues that compose the enzyme active site. The improved resolution of the lyngbyastatin 7–elastase complex provided better insights into key molecular interactions with the enzyme. The cocrystal structure of porcine pancreatic elastase and lyngbyastatin 7 indicated that these compounds act as substrate mimics, with the Abu moiety and the N-terminal residues occupying subsites S1 to S4. They exploit the same binding sites occupied by FR901277 and scyptolin, and the orientation of the macrocyle of these three compounds is also comparable (Figure 3A–C). The ethylidene moiety of the Abu unit in subsite S1 contributes a non-bonded interaction with Ser203 and within distances for CH/π interaction (Figure 3D–E), as previously hypothesized for FR901277.[17] It also forms hydrogen bonds with Gly201 and Ser222, and an indirect hydrogen bond with Thr44 via a water molecule. The cocrystal structure did not show covalent bond formation between the Abu moiety of lyngbyastatin 7 and elastase or hydrolytic cleavage of the macrocyle.

Lyngbyastatin 7 showed extensive hydrogen bonding and van der Waals interactions with elastase and several water molecules in the active site (Figure 3D). The difference in antiproteolytic activity between the *N*-Me-Phe containing compounds (**1**–**3**) with their corresponding *N*-Me-Tyr congeners (**4**–**6**) was evaluated in the context of the cocrystal structure. The OH group of *N*-Me-Tyr forms hydrogen bonds with three water molecules. Val to Ile substitution in the macrocycle did not cause a significant difference in antiproteolytic activity and, based on the cocrystal structure, this moiety is indeed not close to any amino acid residues of elastase for interaction. Comparison of the antiproteolytic activity of compound **5**, lyngbyastatins 4 and 7–9, which all bear exactly the same macrocycle, indicated the contribution of the pendant side chain in modulating the antiproteolytic activity of these elastase inhibitors. Lyngbyastatins 8 and 9 are less potent, with IC_{50}s of 120–210 nM,[8] suggesting that the presence of mainly hydrophobic residues in the pendant side chain is unfavorable. The preference for a polar group in the pendant side chain is supported by the cocrystal structure, wherein the Gln moiety of lyngbyastatin 7 participates in indirect hydrogen bonding with Gln200 and Ser225, via a water molecule; a molecular interaction is not possible with nonpolar moieties in the pendant side chain. The side chain carbonyl of the Gln moiety of lyngbyastatin 7 also participates in a network of intramolecular hydrogen bonding interaction involving an active site water molecule, C=O (Thr) and C=O (Ahp) (Figure 3F). This interaction has not been previously demonstrated and suggests the novelty of having a Gln or related moiety at this position. A linear terminal unit in the pendant side chain appears to be preferable, as the hexanoic acid of lyngbyastatin 7 displays a perfect fit to the elastase binding pocket and also participates in nonbonded interactions with Val103 and Arg226.

Cytoprotective Effects of Compound 1 Against Elastase-Induced Antiproliferation and Apoptosis

We utilized the bronchial epithelial cell line BEAS-2B, a SV-40 transformed cell line that maintains epithelial cell characteristics, as a model system.[19] We challenged these cells with disease-relevant concentrations of exogenous elastase and tested if compound **1** was able to prevent the toxicity by elastase, which showed both a dose- and time-dependent antiproliferative effect based on MTT assay, with IC_{50} values of 77.5 ± 4.9 nM at 24 h (Figure 4A). Compound **1** dose-dependently protected the cells, causing a shift in the IC_{50} of elastase (Figure 4B). The ordinarily toxic concentrations of elastase had little effect on cell viability when **1** was coadministered. At concentrations of 1 or 10 μM compound **1**, cell viability in elastase co-treated cells was >75%. Sivelestat was also protective but required higher concentration (100 μM) to completely negate elastase-induced cytotoxicity (Figure 4C). In addition, **1** did not significantly affect the proliferation of BEAS-2B cells even up to a concentration of 100 μM (Figure 4D) when co-administered with either the solvent control or 100 nM elastase, thus providing a wide therapeutic window at least in cultured cells.

To determine the possible role of apoptosis in the observed antiproliferative effect of elastase, we assessed caspase 3/7 activity of BEAS-2B cells. Increased pro-apoptotic activity was observed upon 12–24 h incubation with 100 nM elastase (Figure 4E), paralleling with the onset of cell viability changes associated with elastase (Figure 4A). Addition of a caspase 3 inhibitor abrogated the observed increase in caspase 3/7 activity from elastase treatment (Figure 4E). Furthermore, treatment of BEAS-2B cells with the caspase 3 inhibitor also caused significant protection from elastase-induced antiproliferation. However, protection was incomplete, which suggests that elastase also reduces cell viability through mechanisms other than apoptosis(Figure 4C). Addition of ≥100 nM compound **1** lowered the caspase 3/7 activity in elastase-treated cells and shifted the EC_{50} of elastase in activating caspases (Figure 4F). Thus, compound **1** counteracted both pro-apoptotic and antiproliferative effects of elastase.

Cytoprotective Effects of Symplostatin 5 (1) Against Elastase -Induced Cell Detachment and Morphological Change

A morphological change of BEAS-2B cells from an epithelial to a rounded and retracted appearance was the most obvious and immediate cellular event that occurred following elastase treatment (Figure 5A). This effect of elastase was observed within 2–3 h, and the early onset suggests that this was independent of cell death. Cells incubated with elastase at 3 and 6 h remained viable, as assessed by MTT and trypan blue staining, despite the obvious change in cell morphology. Furthermore, caspase 3 inhibitor pre-treated cells showed the same rounded appearance (Supporting Information, Figures S1–S4). Compound **1** and sivelestat both dose-dependently prevented elastase-induced cell morphology change (Figure 5A), although sivelestat required a higher concentration during longer incubation periods (12 and 24 h) (Supporting Information, Figures S3, S4), consistent with results from cell viability assays (Figure 4C). Elastase caused a three-fold increase in cell detachment from the collagen base matrix and neighboring cells after 12 h, which was dose-dependently prevented by **1** (Figure 5B). At a concentration of 10 μM of compound **1**, elastase was unable to cause desquamation.

Sivelestat also showed the same cytoprotective effect but again only at higher concentration (100 μM). The ability of elastase to induce cell detachment and morphology change reflects its canonical role in degrading components of the extracellular matrix such as collagen, fibronectin, and elastin and also implicates its effects on cell adhesion molecules. This role of elastase is also dependent on its proteolytic activity as evidenced by abrogation via small molecule inhibition using compound **1** and sivelestat, but not with the caspase inhibitor.

Adhesion molecules such as the immunoglobulin-like cell adhesion molecules (ICAM-1, -2, -3, VCAM, PECAM), integrins, selectins and cadherins are located on the cell surface, are involved in cell and extracellular matrix attachment and also function to modulate leukocyte adhesion and migration, a process essential to progression of inflammation.[20] ICAM-1 is a key regulator of cell-cell adhesion and exists as a membrane-bound protein (mICAM-1) that can be cleaved to generate soluble ICAM-1 (sICAM-1) which is liberated into the medium.[21] sICAM-1 is increased with inflammation and cardiovascular disease and serves as a biomarker.[22,23]

To determine the possible effects of elastase on total ICAM-1 levels in bronchial epithelial cells, culture medium and whole cell lysates were collected after 6 h. sICAM-1 in culture supernatants was quantified by AlphaLisa® and reflects accumulated amount over time. mICAM-1 in whole cell lysates was assessed by immunoblotting and provides a snapshot of the remaining membrane-bound form at the specific timepoint. Media from elastase-challenged cells contained significantly increased sICAM-1 level, which was dose-dependently decreased by cotreatment with ≥1 μM compound **1** (Figure 5C). Elastase-treated cells had lower mICAM-1 amounts at 6 h (Figure 5C), which suggested that the sICAM-1 liberated into culture medium may be generated from the ectodomain shedding of mICAM-1 due to the proteolytic activity of elastase. Inhibition of the proteolytic activity of elastase by cotreatment with **1** caused retention of mICAM-1, thus confirming the role of elastase activity on this cellular event (Figure 5C). Sivelestat also showed a similar effect on sICAM-1 and mICAM-1 levels in response to elastase. This inverse relationship is consistent with sICAM-1 levels in the culture medium and provided internal validation of the direct effects of elastase with the proteolytic cleavage of ICAM-1. Conversely, *ICAM1* transcript levels were not significantly modulated in this cell type as assessed by reverse transcription followed by real-time quantitative polymerase chain reaction (RT-qPCR) (Supporting Information, Figure S5). Taken together, this data further supported the role of elastase as a sheddase, which posttranslationally modifies the membrane-bound form by proteolytic processing to the soluble form.

Attenuation of Global Transcript Changes Induced by Elastase

Elastase has been demonstrated to induce changes in transcript levels of pro-inflammatory cytokines, adhesion molecules and chemokines in vitro, mostly mediated by an NF-κB-dependent pathway.[24–26] The expression of NF-κB-inducible genes is preceded by degradation of cytosolic IκB and nuclear translocation of p65.[27] To determine the possible changes in transcript levels in elastase and elastase+compound **1** treatments, the amount of cytosolic IκB and nuclear p65 was assessed by immunoblotting and ELISA, respectively. Elastase caused a strong decrease in IκB level, which was prevented by **1** (Figure 6A). In accord, a significant increase in nuclear translocation was observed 3 h after elastase treatment and attenuated by cotreatment of **1**. This data is indicative of possible transcript changes associated with elastase treatment that may also be modulated by **1**. Microarray profiling using the Affymetrix GeneChip Human Genome U133 plus 2.0 arrays was performed to comprehensively determine global changes in transcript levels in bronchial epithelial cells following elastase treatment. Elastase caused a significant change in expression ($P < 0.05$, fold change > 1.5) of 364 transcripts corresponding to 348 genes (Figures 6B and C, Supporting Information, Table S6).

Elastase affected the expression of signaling molecules including chemokines, cytokines, and receptors, as well as components of the spliceosome, transcription machinery, cell cycle and ubiquitin-mediated proteolysis. In addition, 13% of elastase-inducible genes currently have no annotation of identity and function, suggesting that our analysis may have identified novel target genes of elastase signaling. Also, of the other 87% of genes with known

identity, 30% do not have a clear function in cellular signaling. Aside from the members of the NOD- and MAPK-signaling pathways, the contribution of other elastase-inducible genes to inflammation or downstream cellular effects of elastase has not been clearly established. Upregulation of kinases (e.g., *PTK2*, *MAP2K5*, *SIK2*, *CSNK1A*) and transcription factors (e.g., *ARID1B*, *NFIB*, *RBM14*) may suggest that elastase is promoting cellular signaling by affecting signaling molecules and/or their activation. The contribution of caspase-independent pathways to elastase-mediated cell death may also be discerned, as several positive modulators of the cell cycle were also upregulated by elastase (e.g., *GAS1*, *DAP3*, *DDIT4*).

Importantly, the transcriptional response to elastase was attenuated by co-administration of 10 μM compound **1**. Comparison of the heatmap of significantly modulated transcripts indicated that **1** potently prevented the global effects of elastase (Figure 6B). Compound **1** caused a 20–68 % reduction in transcript levels of elastase-inducible genes including those involved in NOD- and MAPK- signaling pathways which are relevant to inflammation (Figure 6C). Microarray results were validated by measuring expression levels of important pro-inflammatory cytokines *IL1A*, *IL1B* and *IL8* using RT-qPCR. *IL1B* showed the greatest increase in transcript levels at 3 h, which was strongly abrogated by cotreatment with **1** (Figure 6D). Similar results were obtained for *IL1A* and *IL8*. The effects of elastase on mRNA levels of these three pro-inflammatory cytokines were also assessed at 6 h (Figure 6D). The same trend was observed for *IL1B* and *IL8*, while *IL1A* was not significantly affected at this time point. Transcriptome profiling of BEAS-2B cells treated with compound **1** alone enabled us to characterize possible off-target genes of **1** that are independent of elastase (Supporting Information, Table S7). This analysis identified only nine significantly upregulated transcripts corresponding to nine genes, suggesting high specificity of symplostatin 5 (**1**) for elastase also in cells.

Discussion

Marine cyanobacteria are a prolific source of bioactive modified peptides and depsipeptides.[2] The Ahp-bearing cyclic depsipeptides are an interesting class, primarily because of their predominance, structural diversity and potent protease-inhibitory activity. In Nature, these compounds may act as feeding deterrents, digestion inhibitors in herbivores and possibly regulators of the biosynthesis of coexisting secondary metabolites.[28–30] Despite the potent activity in enzyme assays, their potential biomedical applications have not been rigorously explored. Here we report the purification and structure elucidation of new cyclic depsipeptides bearing the modified amino acid residues Ahp and Abu, termed symplostatins 5–10 (**1**–**6**), and evaluated their cellular effects. Although there are more than 100 members of the Ahp-containing cyclic depsipeptides, the contribution of individual structural units to the activity has not been established, apart from the Ahp and the adjacent N-terminal residue (here: Abu). While the synthesis of representative members of this compound class has been accomplished,[31–33] comprehensive SAR studies based on analogue design have not been reported. Furthermore the variability in conditions for enzyme assays limits direct comparison of literature IC_{50} values. We utilized both experimental SAR data and X-ray cocrystallization to establish the relevance of certain units for potent elastase antiproteolytic activity and selectivity. The macrocyclic *N*-Me-Tyr and a polar functionality in the pendant side chain incrementally increase the potency of these nanomolar inhibitors of elastase. It is perhaps surprising that the pendant side chain, which is highly divergent among these compounds, participates in extensive enzyme-inhibitor interaction and highlights Nature's chemical optimization in a combinatorial fashion. The cocrystal structure information obtained here can be utilized to guide improvements in the design of inhibitors, with the possibility of tuning the activity and selectivity through modifications in both the macrocycle and pendant side chain.

Elastase has been implicated in the progression of chronic inflammatory conditions such as COPD, cystic fibrosis, chronic bronchitis, and asthma, due to the protease–antiprotease imbalance leading to significantly increased levels in biofluids and tissues with nanomolar to micromolar concentrations.[11,34] The canonical role of elastase in degrading the extracellular matrix has been documented, as have the stimulating effects of elastase on signaling pathways through direct or indirect receptor activation. The resulting changes in transcript and protein levels have been linked to possible disease progression.[35] The development of elastase inhibitors as therapies for chronic inflammatory conditions has been challenging due to problems with selectivity and efficacy. We aimed to determine the potential utility of symplostatin 5 (**1**) and related compounds in alleviating the cellular effects downstream of elastase release and compared the cellular potency to sivelestat.

Recent reports demonstrated that elastase can activate apoptosis through a proteinase-activated receptor-1 (PAR-1)-dependent pathway that culminates in the upregulation of NF-κB and p53 and subsequent changes in mitochondrial permeability and caspase activation.[36,37] PARs are seven-transmembrane G-protein coupled receptors that are activated by proteases following cleavage of the extracellular N-terminus, which triggers a change in conformation and coupling to the G-protein.[38] Thrombin is a canonical activator of PARs, while elastase has been reported to have varied effects and PAR substrates, depending on the cell type.[39,40] It is unclear whether elastase directly or indirectly activates PARs. Furthermore, the antiproliferative effects of elastase may be mediated by other pathways as well as its cytostatic effect based on the partial cytoprotection using the caspase inhibitor when compared to **1** and sivelestat. It is then evident that the key to maximum abrogation of elastase-mediated antiproliferative effect is disarming its proteolytic activity. The observed cellular effects of elastase on cell detachment and cell death are important clinical hallmarks of asthma and COPD.[41] Neutrophils mainly cause cell detachment, with elastase and cathepsin G degrading a variety of substrates.[42] In a cellular model system, TNF-α and IFN-γ were also shown to induce desquamation and may function together with serine proteases.[43] Furthermore, lung biopsies of patients indicated that detachment and apoptosis may be related, with the initial sites of cell detachment showing increased apoptotic cells.[43] Cell death has been linked, in addition to persistent inflammation, to contribute to the severity of COPD.[44] Excessive apoptosis is proposed to exacerbate lung disease by preventing re-epithelialisation, development of apoptotic resistance leading to fibrosis and ineffective removal of apoptotic cells, resulting in a persistent inflammatory state.[45]

While elastase-mediated activation of caspases has been related to cell surface receptors, we additionally demonstrated that it can proteolytically process ICAM-1, a critical cell surface receptor that controls cell-cell adhesion, known to be affected by elastase at both the transcript and protein levels in endothelial cells.[25] Purified elastase and sputum samples from cystic fibrosis patients with significant proteolytic activity were shown to induce cleavage of ICAM-1, independent of cell surface expression.[46,47] Aside from controlling cell-cell adhesion, mICAM-1 also binds to leukocytes via the LFA-1 receptor, and its normal expression is required for immune defense.[21] Shedding of mICAM-1 is proposed to serve as a rapid mechanism to regulate leukocyte adhesion and/or promote signal transduction, although it has not been fully elucidated.[48] Our profiling of the transcriptome of bronchial epithelial cells in response to elastase, with or without **1** and vehicle control treatments, indicated that this enzyme upregulates the expression of specific genes. Comprehensive profiling enabled us to identify *IL1B* as the major pro-inflammatory cytokine induced by elastase. Although *IL8* has been reported to be upregulated by elastase in vitro,[24,49,50] our microarray analysis indicated that this gene is less inducible compared to *IL1B*. IL-1β is a key pro-inflammatory cytokine and has increased activity in both COPD and asthma, causing significant airway remodeling and pulmonary inflammation in animal

models, and thus serves as an important biomarker for elastase-mediated cellular effects.[51,52] The expression of IL-1β in elastase-treated animals has been demonstrated to occur via an IL1R1/MyD88 pathway, thus further implicating the role of this enzyme in receptor activation.[52] We also demonstrated that elastase has a broad effect on the transcriptome, and our identification of other elastase target genes may open up new avenues towards the understanding of the physiological and pathological roles of this enzyme.

The ability of symplostatin 5 (**1**) to specifically prevent these hallmarks of disease by blocking elastase activity in both short- and long-term periods indicates that this class of compounds, even though not forming a covalent bond with elastase, lastingly inhibits the enzyme. It displayed a dual mechanism in modulating the cellular effects of elastase by inhibiting the proteolytic processing of direct protein targets of elastase, as well as attenuating the transcriptional responses. In contrast, sivelestat required higher concentration to prevent the long-term effects of elastase, suggesting a saturating condition needed for complete inhibition of elastase. Sivelestat (Figure 1) has a distinct mechanism from compound **1**; it acylates the active site Ser residue of elastase with a pivalyl moiety.[53] This binding is chemically reversible, regenerating the active elastase after deacylation.

Conclusion

We have demonstrated that novel cyanobacterial cyclodepsipeptides can potently inhibit the proteolytic activity of elastase, thereby preventing the downstream cellular effects of this serine protease in a bronchial epithelial model system. Compound **1** alleviated elastase-induced changes in cell viability, apoptosis, cell detachment and alterations in levels of the adhesion molecule ICAM-1, activation of transcription factor NF-κB and global transcriptome changes. At the same time, **1** did not show any cytotoxic effects on bronchial epithelial cells, offering a remarkable therapeutic window. Compound **1** showed equipotent activity as sivelestat in enzyme inhibition and short-term cellular assays. However, **1** showed higher potency in longer-term assays and successfully alleviated several clinical hallmarks of chronic inflammatory diseases such as excessive sICAM-1 production, expression of pro-inflammatory cytokines *IL1A*, *IL1B* and *IL8* and increased cell death and desquamation. Establishment of the molecular basis and biomarkers for elastase inhibition can aid in the design of second-generation inhibitors that are potent, selective and cytoprotective against both short-and long-term effects of elastase.

Materials and Methods

General Experimental Procedures

Optical rotations were measured on a Perkin-Elmer 341 polarimeter. UV spectra were recorded on SpectraMax M5 (Molecular Devices). ^{1}H and 2D NMR spectra were recorded in DMSO-d_6 on a Bruker Avance II 600 MHz spectrometer equipped with a 5-mm TXI cryogenic probe using residual solvent signals [(DMSO-d_6: δ_H 2.50; δ_C 39.5)] as internal standards. HSQC and HMBC experiments were optimized for $^1J_{CH}$ = 145 and $^nJ_{CH}$ = 7 Hz, respectively. TOCSY experiments were done using a mixing time of 100 ms. HRESIMS data was obtained using an Agilent LC-TOF mass spectrometer equipped with an APCI/ESI multimode ion source detector. LRESIMS measurements and MRM analysis were done on an ABI 3200Q TRAP. Compounds have purity ≥ 95% based on HPLC.

Biological Material

The red *Symploca* sp. cyanobacterium was collected by hand from Cetti Bay, Guam. Samples were kept frozen at −20 °C after collection. A voucher specimen preserved in

formaldehyde is deposited in the University of Guam Herbarium and at the Smithsonian Marine Station, Fort Pierce, FL. Frozen cyanobacterium samples were lyophilized prior to extraction.

Extraction and Isolation

The freeze-dried cyanobacterium was extracted with EtOAc–MeOH (1:1) to yield the nonpolar extract. This was partitioned between hexanes and 80% aqueous MeOH, the latter concentrated under reduced pressure and further partitioned between *n*-BuOH and H_2O. The *n*-BuOH fraction was concentrated to dryness and chromatographed on Si gel eluting first with CH_2Cl_2, followed by increasing concentrations of *i*-PrOH, while after 100% *i*-PrOH, increasing gradients of MeOH were used.

The fraction collected from 50% *i*-PrOH elution (Si column) was purified by C18 column chromatography eluting with 25%, 50%, 75% and 100% MeOH in H_2O. The fraction from 50% MeOH was further purified using semipreparative reversed-phase HPLC (Phenomenex Synergi-Hydro RP, 4 μm; flow rate, 2.0 mL/min) using a linear gradient of MeCN–H_2O (25%–100% MeOH in 30 min and then 100% MeCN for 10 min) to yield compounds **5** (t_R 17.8 min, 1.0 mg), **4** (t_R 19.0 min, 1.0 mg) and **6** (t_R 36.6 min, 0.3 mg). The 75% MeOH fraction was purified using the same HPLC conditions to yield compounds **2** (t_R 23.8 min, 3.5 mg), **1** (t_R 24.0 min, 7.0 mg) and **3** (t_R 25.3 min, 1.0 mg).

Enantioselective Analysis

Portions of **1**–**6** (100 μg) were acid-hydrolyzed (200 μL 6 N HCl, 110 °C, 20 h), the product mixtures dried and reconstituted in 100 μL H_2O. The absolute configurations of the amino acids (Ile, Val, *N*-Me-Tyr, *N*-Me-Phe, Phe, Thr) were determined by enantioselective HPLC-MS [column, Chirobiotic TAG (250 × 4.6 mm), Supelco; solvent, MeOH–10 mM NH_4OAc (40:60, pH 5.30); flow rate, 0.5 mL/min; detection by ESIMS in positive ion mode (MRM scan)]. The retention times (t_R, min; MRM ion pair) of the authentic amino acids were as follows: L-Val (7.8; 118→72), D-Val (13.7); *N*-Me-L-Phe (22.7; 180→134), *N*-Me-D-Phe (40.4); L-Phe (12.1; 166→103), D-Phe (17.5); *N*-Me-L-Tyr (18.8; 196→77), *N*-Me-D-Tyr (35.4); L-Thr (6.8; 120→74), L-*allo*-Thr (7.2), D-Thr (8.0), D-*allo*-Thr (10.2). In order to separate Ile isomers, the mobile phase was modified to MeOH–10 mM NH_4OAc (90:10, pH 5.65) while keeping the same chromatographic conditions. The retention times of authentic standards were as follows: L-Ile (10.4; 132→86), L-*allo*-Ile (11.2), D-*allo*-Ile (20.1), D-Ile (22.2).

The acid hydrolysates of **1**–**6** showed retention times at 6.8 and 12.1 min corresponding to L-Thr and L-Phe, respectively. L-Val (t_R 7.8 min) was detected in the acid hydrolysates of **1**, **2**, **4**, and **5**. The acid hydrolysates of **1**, **3**, **4** and **6** showed a peak corresponding to L-*allo*-Ile (t_R 11.2 min). **3** and **6** had an additional peak corresponding to L-Ile (t_R 10.4 min). *N*-Me-L-Phe (t_R 22.7 min) was detected in the acid hydrolysate of **1**–**3**, while *N*-Me-L-Tyr (t_R 18.8 min) was present in the acid hydrolysate of **4**–**6**.

The modified (2*S*)-2-*O*-Me glyceric acid residue was prepared using L-Ser (50 mg), isoamyl nitrite (70.5 μL), glacial CH_3COOH (17.2 μL), $MgSO_4$ (60 mg) and anhydrous MeOH (1 mL). The mixture was heated at 110 °C for 4 h, cooled down to room temperature and filtered. The filtrate was evaporated to dryness under N_2 to yield (2*S*)-2-*O*-Me glyceric acid. The same procedure was employed to prepare (2*R*)-2-*O*-Me glyceric acid from D-Ser. LRESIMS and ^{13}C NMR spectrum for (2*S*)-2-*O*-Me glyceric acid and (2*R*)-2-*O*-Me glyceric acid were in agreement with reported literature values.[54]

The absolute configuration of Glu and 2-*O*-Me glyceric acid was also determined using HPLC-MS [column, Chirobiotic TAG (250 × 4.6 mm), Supelco; solvent, MeOH–10 mM NH_4OAc (40:60, pH 5.30); flow rate, 0.5 mL/min] with detection in the negative ion mode (MRM). The retention times of the authentic standards (t_R, min; MRM pair): L-Glu (5.1; 146→102), D-Glu (6.1), (2*S*)-2-*O*-Me glyceric acid (6.1; 119→89), (2*R*)-2-*O*-Me glyceric acid (6.6). Compound **1** was oxidized using CrO_3 and hydrolyzed using 6 N HCl (110 °C, 20 h) to convert Ahp to Glu. The oxidation product's acid hydrolysate showed a peak at 5.1 min corresponding to L-Glu. The acid hydrolysate of **1** yielded a peak for (2*R*)-2-*O*-Me glyceric acid (t_R 6.6 min).

Symplostatin 5 (1): colorless, amorphous solid; $[\alpha]^{20}_D$ –3.6 (*c* 0.14, MeOH); UV (MeOH); λ_{max} (log ε) 210 (4.49); ^{1}H NMR, ^{13}C NMR, COSY, and HMBC data, see Table 1; HRESIMS *m/z* 1044.3981 $[M + Na]^+$ (calcd for $C_{47}H_{64}N_7O_{15}SNa$, 1044.3971).

Symplostatin 6 (2): colorless, amorphous solid; $[\alpha]^{20}_D$ –5.2 (*c* 0.26, MeOH); UV (MeOH); λ_{max} (log ε) 204 (4.49); ^{1}H NMR and ^{13}C NMR data, see Table S1; HRESIMS *m/z* 1030.3815 $[M + Na]^+$ (calcd for $C_{46}H_{62}N_7O_{15}SNa$, 1030.3815).

Symplostatin 7 (3): colorless, amorphous solid; $[\alpha]^{20}_D$ –14 (*c* 0.15, MeOH); UV (MeOH); λ_{max} (log ε) 202 (4.48); ^{1}H NMR and ^{13}C NMR data, see Table S2; HRESIMS *m/z* 1058.4104 $[M + Na]^+$ (calcd for $C_{48}H_{66}N_7O_{15}SNa$, 1058.4128).

Symplostatin 8 (4): colorless, amorphous solid; $[\alpha]^{20}_D$ –6.7 (*c* 0.09, MeOH); UV (MeOH); λ_{max} (log ε) 210 (4.13); ^{1}H NMR and ^{13}C NMR data, see Table S3; HRESIMS *m/z* 1060.3941 $[M + Na]^+$ (calcd for $C_{46}H_{64}N_7O_{16}SNa$, 1060.3920).

Symplostatin 9 (5): colorless, amorphous solid; $[\alpha]^{20}_D$ –3.5 (*c* 0.10, MeOH); UV (MeOH); λ_{max} (log ε) 204 (3.94); ^{1}H NMR and ^{13}C NMR data, see Table S1; HRESIMS *m/z* 1046.3747 $[M + Na]^+$ (calcd for $C_{46}H_{64}N_7O_{16}SNa$, 1046.3764).

Symplostatin 10 (6): colorless, amorphous solid; $[\alpha]^{20}_D$ –3.3 (*c* 0.03, MeOH); UV (MeOH); λ_{max} (log ε) 200 (5.24); ^{1}H NMR and ^{13}C NMR data, see Table S2; HRESIMS *m/z* 1074.4060 $[M + Na]^+$ (calcd for $C_{48}H_{66}N_7O_{16}SNa$, 1074.4077).

In Vitro Protease Assay

Porcine pancreatic elastase (Elastin Products Company, Owensville, MO) was dissolved in Tris-HCl (pH 8.0) to give a concentration of 75 μg/mL. Test compounds (1 μL, DMSO), 5 μL elastase solution and 79 μL Tris-HCl (pH 8.0) were pre-incubated at room temperature for 15 min in a 96-well microtiter plate. At the end of the incubation, 15 μL substrate solution were added [2 mM *N*-succinyl-Ala-Ala-Ala-*p*-nitroanilide (Sigma-Aldrich, St. Louis, MO) in Tris-HCl, pH 8.0] to each well, and the reaction was monitored by recording the absorbance at 405 nm every 30 s. The inhibitory activity against human neutrophil elastase was also determined using the same procedure with minor modifications, using 100 μg/mL human neutrophil elastase (Elastin Products Company) and 2 mM *N*-(OMe-succinyl)-Ala-Ala-Pro-Val-*p*-nitroanilide (Sigma-Aldrich), both prepared in 0.1 M Tris-NaCl buffer (pH 7.5). Enzyme activity was determined by calculating the initial slope of each progress curve, expressed as a percentage of the slope of the uninhibited reaction. Antiproteolytic activity against bovine (100 μg/mL) and human (50 μg/mL) pancreatic chymotrypsin (Sigma-Aldrich) were assessed using the substrates *N*-succinyl-Gly-Gly-Phe-*p*-nitroanilide (Sigma-Aldrich) and *N*-succinyl-Ala-Ala-Pro-Phe-*p*-nitroanilide (Sigma-Aldrich), respectively. In brief, the reaction buffer (39 μL), enzyme (10 μL) and inhibitor (1 μL) were incubated for 30 min at room temperature before the addition of 50 μL of

substrate. The absorbance was monitored at 405 nm. Enzyme activity in each well was calculated based on the slope of the reaction curve compared to that of the solvent control.

For high-throughput screening, enzyme and inhibitor [compound **1** or lyngbyastatin 7] were incubated for 15 min in the reaction buffer before the addition of the substrate. The reaction was monitored for 2 h and the initial linear portion of the slope was analyzed. Detailed information on the enzymes, substrates, reaction buffers and detection conditions are given in the Supporting Information (Table S4).

Cocrystallization of Lyngbyastatin 7 with Porcine Pancreatic Elastase

A 10-μL aliquot of high purity porcine pancreatic elastase:lyngbyastatin 7 solution (3:1) was incubated in a hanging drop setup equilibrated against a 0.42 M sodium sulfate solution. Diffraction data was collected on beamline X6A at the National Synchrotron Light Source (Upton, NY). Diffraction data was processed using HKL2000[55] and the structure was solved by molecular replacement using 2V0B as search model in MOLREP (CCP4).[56,57] The model was refined using REFMAC[58] and COOT.[59] Detailed information on the refinement statistics are provided in the Supporting Information (Table S5). Coordinates are deposited in the Protein Databank with accession number 4GVU.

In vitro Cellular Assays

General Cell Culture Procedure

Bronchial epithelial cells (BEAS-2B, ATCC) were grown in bronchial epithelial basal media (BEBM) (Lonza, Walkersville, MD) supplemented with bronchial epithelial growth factors (Lonza) under a humidified environment with 5% CO_2 at 37 °C. All culture plates and flasks were coated with collagen before use.

Cell Viability Assay

BEAS-2B (5,000/well) cells were seeded in collagen-coated 96-well plates and treated with varying concentrations of elastase or vehicle (40% sodium acetate in BEBM) after 24 h of seeding. These were co-treated with varying doses of either symplostatin 5 (**1**) or sivelestat (Sigma-Aldrich) or with DMSO. The cells were incubated for an additional 24 h before the addition of the MTT reagent. Cell viability was measured according to the manufacturer's instructions (Promega, Madison, WI). IC_{50} calculations were done by GraphPad Prism 5.03 based on duplicate experiments.

Cell Detachment and Morphology Change

BEAS-2B cells were seeded in 6-cm dishes. The cells were treated with vehicle+DMSO, elastase+DMSO and elastase+inhibitor. Brightfield photographs were taken at 3 h, 6 h, 12 h and 24 h using a Nikon Eclipse T*i*-U microscope (10× magnification). Media were collected after 12 h and the detached cells were pelleted by centrifugation. Adherent cells were collected by trypsinization and pelleted afterwards. Cell pellets were resuspended in fresh culture medium containing 0.04% trypan blue. A 10-μL aliquot was utilized for cell counting using a hemacytometer. Percent detachment was calculated based on the ratio of the detached cells and total number of cells. Graphs and data analysis were performed using the Prism software and analyzed using ANOVA followed by Dunnett's t-test.

Caspase Activation Measurement

BEAS-2B cells were prepared similar to the cell viability assay. Cells were treated 24 h post seeding with vehicle+DMSO, elastase+DMSO, elastase+compound **1**. In addition, BEAS-2B cells were pre-incubated with 10 μM Z-D(OMe)E(OMe)VD(OMe)-FMK, a

caspase 3 inhibitor (Calbiochem, Billerica, MA), for 1 h prior to addition of varying concentrations of elastase. At the end of the 24 h incubation period, the medium was replaced with fresh BEBM and incubated for 10 min at room temperature. The caspase reagent was prepared according to the manufacturer's instruction (Promega) and was added to each well and incubated for 10 min to ensure complete cell lysis. Luminescence was measured and the relative caspase 3/7 activity of elastase and elastase+symplostatin 5 (**1**) treated cells were compared to the control.

Measurement of sICAM-1 Levels

BEAS-2B cells (60,000/well) were seeded in collagen-coated 24-well plates. After overnight incubation, the medium was replaced with supplement-free media and the cells were further incubated for 24 h. At the end of the incubation period, cells were replenished with new supplement-free medium prior to treatment. Cells were treated with elastase together with DMSO or varying concentrations of symplostatin 5 (**1**) dissolved in DMSO. Control cells were treated with DMSO (1%) and sodium acetate in supplement-free medium (4%). The cells were incubated and culture supernatants were collected after 6 h. sICAM-1 levels were determined using ICAM-1 AlphaLisa® Kit (PerkinElmer, Waltham, MA) according to the manufacturer's instruction. Graphs and data analysis were performed using the Prism software and analyzed using ANOVA followed by Dunnett's t-test.

Immunoblot Analysis of mICAM-1 Levels

BEAS-2B cells (150,000/well) were grown in collagen-coated 6-cm tissue culture dishes. The supplemented medium was replaced with BEBM after overnight incubation and further left to acclimatize for 24 h in supplement-free medium. Cells were replenished with fresh BEBM and treated with elastase together with DMSO or varying concentrations of compound **1**. Cells were harvested and lysed with PhosphoSafe lysis buffer (Novagen, Madison, WI) after 6 h. The protein concentration of whole cell lysates was measured with the BCA Protein Assay kit (Pierce Chemical, Rockford, IL). Equal amounts of protein were separated by SDS-polyacrylamide gel electrophoresis (4–12%), transferred to polyvinylidene difluoride (PVDF) membranes, probed with anti-ICAM-1 antibody (Abcam, Cambridge, MA) and detected with the SuperSignal West Femto Maximum Sensitivity Substrate (Pierce). The immunoblots were stripped by heating in a water bath (90 °C) and reprobed with anti-β-actin antibody (Cell Signaling, Danvers, MA) to confirm equal protein loading.

Isolation of Nuclear and Cytoplasmic Proteins

Cells (150,000/well) were seeded in collagen-coated 10-cm dishes. Culture media were replaced prior to treatment with elastase and/or elastase+compound **1**. After varying incubation times (1, 3, and 6 h), the culture supernatant was collected and phosphate-buffered saline supplemented with 1.5× protease inhibitor cocktail (Roche, Indianapolis, IN) was added to each dish. The cells were lifted from the culture dish using a cell scraper and pelleted by centrifugation (300*g*) at 4 °C for 5 min. Cytoplasmic proteins were collected using the NE-PER® Cytoplasmic Extraction Reagent (Thermo Scientific, Rockford, IL) according to the manufacturer's instruction. After collection of the cytoplasmic fraction, the insoluble pellet was washed with PBS, centrifuged for 1 min and the supernatant was discarded. Nuclear proteins were isolated from the insoluble pellet. All extracts were incubated on ice, and protein concentration was determined using the BCA reagent (Pierce).

Measurement of IκBα Degradation and NF-κB p65 Translocation

IκBα degradation was assessed by immunoblotting of the collected cytoplasmic proteins. Equal amounts of the cytoplasmic fraction was loaded and separated in a 4–12% Bis-Tris

HCl gel, transferred on a PVDF membrane and probed with an anti-IκBα antibody (Cell Signaling) and detected with SuperSignal Femto Max reagent (Pierce). The blots were stripped after detection by incubating at 90 °C and subsequently probed with anti-β-tubulin (Cell Signaling) to assess protein loading. NF-κB p65 translocation was measured using the TransAM NF-κB Chemi p65 kit (Active Motif, Carlsbad, CA) and done according to the manufacturer's instruction. In brief, equal amounts of the nuclear protein were prepared in the TransAM complete lysis buffer. The nuclear extracts were added to oligonucleotide coated plates containing complete binding buffer. This was allowed to incubate at room temperature with mild agitation for 1 h, washed and incubated with NF-κB p65 primary antibody for 1 h. The wells were washed and subsequently incubated for 1 h with anti-rabbit horseradish peroxidase-conjugated antibody. The chemiluminescent reagent was added after the incubation period and luminescence was measured. The relative NF-κB p65 translocation of elastase and elastase+compound **1** treated cells were compared to the control. To ascertain the specificity of the measured activity, elastase treatments were also incubated with wild-type oligonucleotide AM20 which prevented NF-κB p65 binding to the oligonucleotide probe immobilized on the plate. Each experiment was performed in triplicate. Graphs and data analysis were performed using the Prism software and analyzed using ANOVA followed by Dunnett's t-test.

RNA Isolation and Reverse Transcription

A total of 1.2×10^6 BEAS-2B cells were seeded in 10-cm dishes and incubated further for 24 h in supplement-free medium prior to treatment. RNA was isolated at 3 and 6 h post treatment using RNeasy mini kit (QIAGEN, Valencia, CA). Total RNA was quantified by UV absorbance. From 2 μg total RNA, cDNA synthesis was done using SuperScript II Reverse Transcriptase (Invitrogen, Carlsbad, CA) and oligo$(dT)_{12–18}$ (Invitrogen).

Real-time Quantitative Polymerase Chain Reaction (qPCR)

qPCR after reverse transcription (RT-qPCR) was performed on a 25 μL reaction solution containing a 1.5 μL aliquot of cDNA, 12.5 μL TaqMan gene expression assay mix, 1.25 μL of 20× TaqMan gene expression assay mix and 9.25 μL RNase-free water. qPCR was carried out on an ABI 7300 sequence detection system using the thermocycler program: 2 min at 50 °C, 10 min at 95 °C, and 15 s at 95 °C (40 cycles) and 1 min at 60 °C. Each experiment was performed in triplicate. *IL1A* (Hs00174092_m1), *IL1B* (Hs01555410_m1), and *IL8* (Hs00174103_m1) were used as target genes, while *GAPDH* (Hs02758991_g1) was used as endogenous control. Graphs and data analysis were performed using the Prism software and analyzed using ANOVA followed by Dunnett's t-test.

Transcriptome Profiling

RNA was analyzed using a NanoDrop Spectrophotometer and Agilent 2100 Bioanalyzer to determine the RNA concentration and quality, respectively. RNA samples were processed using the GeneChip 3′ IVT Express kit (Affymetrix, Santa Clara, CA) according to the manufacturer's instruction. In brief, 250 ng RNA were used for cDNA synthesis by reverse transcription and the cDNA was utilized as a template for the biotin-labeled RNA prepared by in vitro transcription reaction. The labeled RNA was further purified, fragmented and hybridized with rotation at 45 °C for 16 h to the Affymetrix GeneChip Human Genome U133 plus 2.0 arrays. The arrays were washed and stained using the GeneChip Hybridization Wash and Stain kit on an Affymetrix Fluidics Station 450. The chips were scanned using a GeneChip 7G Scanner. Analysis of the microarray data was done according to the reported method.[60] Raw data was normalized using the Robust Multichip Analysis approach and statistical analysis was done using the Bioconductor statistical software and R program. The probe set's detection call was estimated using the Wilcoxon signed rank-based

algorithm. Probe sets that are absent in all of the study samples were removed from further analyses. Differential expression analysis was performed using a linear modeling approach and the empirical Bayes statistics as implemented in the limma package of the R software. The *P* values obtained were controlled for multiple testing (false discovery rate) using the Benjamini-Hochberg method. *P* value and fold induction were calculated. Differentially expressed transcripts were ranked by *P* values, and $P < 0.05$ and fold induction >1.5 were considered at a statistically significant level. Hierarchical clustering of the data was computed on log-transformed and normalized data by using complete linkage and Pearson correlation distances. Computation and visualization were done with R packages. Gene ontology was performed using the DAVID Bioinformatics Resources 6.7.[61,62] The transcriptome data is deposited in NCBI's Gene Expression Omnibus with accession number GSE41600.

Supplementary Material

Refer to Web version on PubMed Central for supplementary material.

Acknowledgments

We are grateful to J. Rocca (AMRIS) for assistance in obtaining the NMR spectra, J. Quiñata of the Cetti Bay Ecostation (Agat, Guam) for collection access, X. Han and J. Yao (Bioinformatics Division, ICBR at UF) for assistance with the microarray analysis. This is contribution #901 from the Smithsonian Marine Station at Fort Pierce. This research was supported by the National Institutes of Health, NIGMS [Grant P41GM086210].

List of Abbreviations

Abu	2-amino-2-butenoic acid
Ahp	3-amino-6-hydroxy-2-piperidone
ANOVA	analysis of variance
ARID1B	AT rich interactive domain 1B
BCA	bicinchoninic acid
BEBM	bronchial epithelial basal medium
CSNK1A	casein kinase 1, alpha
DAP3	death associated protein 3
DDIT4	DNA-damage-inducible transcript 4
GAPDH	glyceraldehyde 3-phosphate dehydrogenase
GAS1	growth arrest-specific 1
HNE	human neutrophil elastase
IκBα	NF-κB inhibitor α
ICAM-1	intercellular adhesion molecule-1
IFN-γ	interferon γ
IL1A	interleukin 1A
IL1B	interleukin 1B
IL1R1	interleukin receptor, type 1
IL8	interleukin 8

IVT	in vitro transcription
MAP2K5	mitogen-activated protein kinase kinase 5
mICAM-1	membrane-bound intercellular adhesion molecule-1
MRM	multiple reaction monitoring
MTT	3-(4,5-dimethylthiazol-2-yl)-2,5-diphenyltetrazolium bromide
MyD88	myeloid differentiation primary response gene (88)
NFIB	nuclear factor I/B
NOD	nucleotide-binding oligomerization domain
PAR	proteinase-activated receptor
PECAM	platelet endothelial cell adhesion molecule
PTK2	protein tyrosine kinase 2
RBM14	RNA binding motif protein 14
sICAM-1	soluble intercellular adhesion molecule-1
SIK2	salt-inducible kinase 2
VCAM	vascular cell adhesion protein

References

1. Gademann K, Portmann C. Secondary metabolites from marine cyanobacteria: complex structures and powerful bioactivities. Curr Org Chem. 2008; 12:326–341.
2. Tan LT. Filamentous tropical marine cyanobacteria: a rich source of natural products for anticancer drug discovery. J Appl Phycol. 2010; 22:659–676.
3. Chlipala GE, Mo S, Orjala J. Chemodiversity in freshwater and terrestrial cyanobacteria - A source for drug discovery. Curr Drug Targets. 2011; 12:1654–1673. [PubMed: 21561419]
4. Linington RG, Edwards DJ, Shuman CF, McPhail KL, Matainaho T, Gerwick WH. Symplocamide A, a potent cytotoxin and chymotrypsin inhibitor from the marine cyanobacterium *Symploca* sp. J Nat Prod. 2008; 71:22–27. [PubMed: 18163584]
5. Lee AY, Smitka TA, Bonjouklian R, Clardy J. Atomic structure of the trypsin-A90720A complex: a unified approach to structure and function. Chem Biol. 1994; 1:113–117. [PubMed: 9383379]
6. Matern U, Schelberger C, Jelakovic S, Weckesser J, Schulz GE. Binding structure of elastase inhibitor scyptolin A. Chem Biol. 2003; 10:997–1001. [PubMed: 14583266]
7. Taori K, Matthew S, Rocca JR, Paul VJ, Luesch H. Lyngbyastatins 5–7, potent elastase inhibitors from Floridian marine cyanobacteria, *Lyngbya* spp. J Nat Prod. 2007; 70:1593–1600. [PubMed: 17910513]
8. Kwan JC, Taori K, Paul VJ, Luesch H. Lyngbyastatins 8–10, elastase inhibitors with cyclic depsipeptide scaffolds isolated from the marine cyanobacterium*Lyngbya semiplena*. Mar Drugs. 2009; 7:528–538. [PubMed: 20098596]
9. Matthew S, Ross C, Rocca JR, Paul VJ, Luesch H. Lyngbyastatin 4, a dolastatin 13 analogue with elastase and chymotrypsin inhibitory activity from the marine cyanobacterium *Lyngbya confervoides*. J Nat Prod. 2007; 70:124–127. [PubMed: 17253864]
10. Korkmaz B, Horwitz MS, Jenne DE, Gauthier F. Neutrophil elastase, proteinase 3 and cathepsin G as therapeutic targets in human disease. Pharmacol Rev. 2010; 62:726–759. [PubMed: 21079042]
11. Roghanian A, Sallenave J. Neutrophil elastase (NE) and NE inhibitors: canonical and noncanonical functions in lung chronic inflammatory diseases (cystic fibrosis and chronic obstructive pulmonary disease). J Aerosol Med Pulm D. 2008; 21:125–144.

12. Barnes PJ, Stockley RA. COPD: current therapeutic interventions and future approaches. Eur Respir J. 2005; 25:1084–1106. [PubMed: 15929966]
13. Imaki K, Okada T, Nakayama Y, Nagao Y, Kobayashi K, Sakai Y, Mohri T, Amino T, Nakai H, Kawamura M. Non-peptidic inhibitors of human neutrophil elastase: the design and synthesis of sulfonanilide-containing inhibitors. Bioorg Med Chem. 1996; 4:2115–2134. [PubMed: 9022976]
14. Zeiher BG, Artigas A, Vincent J, Dmitrienko A, Jackson K, Thompson BT, Bernard G. for the STRIVE Study Group. Neutrophil elastase inhibition in acute lung injury: results of the STRIVE study. Crit Care Med. 2004; 32:1695–1702. [PubMed: 15286546]
15. Pauwels RA, Buist AS, Calverley PM, Jenkins CR, Hurd SS. Global strategies for the diagnosis, management, and prevention of chronic obstructive pulmonary disease. NHLBI/WHO Global Initiative for Chronic Obstructive Lung Disease (GOLD) Workshop summary. Am J Respir Crit Care Med. 2001; 163:1256–1276. [PubMed: 11316667]
16. Wright JL, Cosio M, Chung A. Animal models of chronic obstructive pulmonary disease. Am J Physiol Lung Cell Mol Physiol. 2008; 295:L1–L15. [PubMed: 18456796]
17. Nakanishi I, Kinoshita T, Sato A, Tada T. Structure of porcine pancreatic elastase complexed with FR901277, a novel macrocyclic inhibitor of elastases, at 1. 6 Å resolution. Bioploymers. 2000; 51:434–445.
18. Bode W, Meyer E Jr, Powers JC. Human leukocyte and porcine pancreatic elastase: X-ray crystal structures, mechanism, substrate specificity, and mechanism -based inhibitors. Biochemistry. 1989; 28:1951–1963. [PubMed: 2655701]
19. Reddel RR, Ke Y, Gerwin BI, McMenamin MG, Lechner JF, Su R, Brash DE, Park J, Rihm JS, Harris CC. Transformation of human bronchial epithelial cells by infection with SV40 or adenovirus-12 SV40 hybrid virus, or transfection via strontium phosphate coprecipitation with a plasmid containing SV40 early region genes. Cancer Res. 1988; 48:1904–1909. [PubMed: 2450641]
20. Ley K, Laudanna C, Cybulsky MI, Nourshargh S. Getting to the site of inflammation: the leukocyte adhesion cascade updated. Nat Rev Immunol. 2007; 7:678–689. [PubMed: 17717539]
21. van de Stolpe A, van der Saag PT. Intercellular adhesion molecule-1. J Mol Med. 1996; 74:13–33. [PubMed: 8834767]
22. Labarrere CA, Nelson DR, Miller SJ, Nieto JM, Conner JA, Pitts DE, Kirlin PC, Halbrook HG. Value of serum-soluble intercellular adhesion molecule-1 for the noninvasive risk assessment of transplant coronary artery disease, posttransplant ischemic events, and cardiac graft failure. Circulation. 2000; 102:1549–1555. [PubMed: 11004146]
23. Ciebiada M, Gorska-Ciebiada M, Gorski P. sICAM-1 and TNF-α in asthma and rhinitis: relationship with the presence of atopy. J Asthma. 2011; 48:660–666. [PubMed: 21838623]
24. Walsh DE, Greene CM, Carroll TP, Taggart CC, Gallagher PM, O'Neill SJ, McElvaney NG. Interleukin-8 up-regulation by neutrophil elastase is mediated by MyD88/IRAK/TRAF-6 in human bronchial epithelium. J Biol Chem. 2001; 276:35494–35499. [PubMed: 11461907]
25. Ishihara K, Yamaguchi Y, Uchino S, Furuhashi T, Yamada S, Kihara S, Mori K, Ogawa M. ICAM-1 signal transduction in cells stimulated with neutrophil elastase. Dig Dis Sci. 2006; 51:2102–2112. [PubMed: 17024574]
26. Geraghty P, Rogan MP, Greene CM, Boxio RMM, Poiriert T, O'Mahony M, Belaaouaj A, O'Neill SJ, Taggart CC, McElvaney NG. Neutrophil elastase up-regulates cathepsin B and matrix metalloprotease-2 expression. J Immunol. 2007; 178:5871–5878. [PubMed: 17442971]
27. Gilmore TD. Introduction to NF-κB: players, pathways, perspectives. Oncogene. 2006; 25:6680–6684. [PubMed: 17072321]
28. Schatz D, Keren Y, Vardi A, Sukenik A, Carmeli S, Börner T, Dittmann E, Kaplan A. Towards clarification of the biological role of microcystins, a family of cyanobacterial toxins. Environ Microbiol. 2007; 9:965–970. [PubMed: 17359268]
29. Matthew S, Ratnayake R, Becerro MA, Ritson-Williams R, Paul VJ, Luesch H. Intramolecular modulation of serine protease inhibitor activity in a marine cyanobacterium with antifeedant properties. Mar Drugs. 2010; 8:1803–1806. [PubMed: 20631871]

30. Schwarzenberger A, Kuster CJ, Elert E. Molecular mechanisms of tolerance to cyanobacterial protease inhibitors revealed by clonal differences in *Daphnia magna*. Mol Ecol. 2012; 0:4898–4911. [PubMed: 22943151]
31. Yokokawa F, Shioiri T. Total synthesis of somamide A, an Ahp (3-amino-6-hydroxy-2-piperidone)-containing cyclic depsipeptide. Tet Lett. 2002; 43:8673–8677.
32. Yokokawa F, Inaizumi A, Shioiri T. Synthetic studies of the cyclic depsipeptides bearing the 3-amino-6-hydroxy-2-piperidone (Ahp) unit. Total synthesis of the proposed structure of micropeptin T-20. Tetrahedron. 2005; 61:1459–1480.
33. Stolze SC, Meltzer M, Ehrmann M, Kaiser M. Development of a solid-phase approach to the natural product class of Ahp-containing cyclodepsipeptides. Eur J Org Chem. 2012; 2012:1616–1625.
34. Vignola AM, Bonanno A, Mirabella A, Riccobono L, Mirabella F, Profita M, Bellia V, Bousquet J, Bonsignore G. Increased levels of elastase and α1-antitrypsin in sputum of asthmatic patients. Am J Respir Crit Care Med. 1998; 157:505–511. [PubMed: 9476865]
35. Lungarella G, Cavarra E, Lucattelli M, Martorana PA. The dual role of neutrophil elastase in lung destruction and repair. Int J Biochem Cell Biol. 2008; 40:1287–1296. [PubMed: 18243764]
36. Suzuki T, Moraes TJ, Vachon E, Ginzberg HH, Huang T, Matthay MA, Hollenberg MD, Marshall J, McCulloch CAG, Abreu MTH, Chow C, Downey GP. Proteinase-activated receptor-1 mediates elastase-induced apoptosis of human lung epithelial cells. Am J Respir Cell Mol Biol. 2005; 33:231–247. [PubMed: 15891109]
37. Suzuki T, Yamashita C, Zemans RL, Briones N, Van Linden A, Downey GP. Leukocyte elastase induces lung epithelial apoptosis via a PAR-1–, NF-κB–, and p53-dependent pathway. Am J Respir Cell Mol Biol. 2009; 41:742–755. [PubMed: 19307610]
38. Macfarlane SR, Seatter MJ, Kanke T, Hunter GD, Plevin R. Proteinase-activated receptors. Pharmacol Rev. 2001; 2001:245–282. [PubMed: 11356985]
39. Coughlin SR. Thrombin signalling and protease-activated receptors. Nature. 2000; 407:258–264. [PubMed: 11001069]
40. Uehara A, Muramoto K, Takada H, Sugawara S. Neutrophil serine proteinases activate human nonepithelial cells to produce inflammatory cytokines through protease-activated receptor 2. J Immunol. 2003; 170:5690–5696. [PubMed: 12759451]
41. Jeffrey PK. Remodeling and inflammation of bronchi in asthma and chronic obstructive pulmonary disease. Proc Am Thorac Soc. 2004; 1:176–183. [PubMed: 16113432]
42. Mendis AHW, Venaille TJ, Robinson BWS. Study of human epithelial cell detachment and damage: effects of proteases and oxidants. Immunol Cell Biol. 1990; 68:95–105. [PubMed: 2200749]
43. Trautman A, Kruger K, Akdis M, Muller-Wenning D, Akkaya A, Brocker E, Blaser K, Akdis CA. Apoptosis and loss of adhesion of bronchial epithelial cells in asthma. Int Arch Allergy Immunol. 2005; 138:142–150. [PubMed: 16179825]
44. Tuder RM, Petrache I, Elias JA, Voelkel NF, Henson PM. Apoptosis and emphysema: the missing link. Am J Respir Cell Mol Biol. 2003; 28:551–554. [PubMed: 12707010]
45. Drakopanagiotakis F, Xifteri A, Polychronopoulos V, Bouros D. Apoptosis in lung injury and fibrosis. Eur Respir J. 2008; 32:1631–1638. [PubMed: 19043009]
46. Champagne B, Tremblay P, Cantin A, St Pierre Y. Proteolytic cleavage of ICAM -1 by human neutrophil elastase. J Immunol. 1998; 161:6398–63405. [PubMed: 9834131]
47. Robledo O, Papaioannou A, Ochietti B, Beauchemin C, Legault D, Cantin A, King PD, Daniel C, Alakhov VY, Potworowski EF, St-Pierre Y. ICAM-1 isoforms: specific activity and sensitivity to cleavage by leukocyte elastase and cathepsin G. Eur J Immunol. 2003; 33:1351–1360. [PubMed: 12731061]
48. Garton KJ, Gough PJ, Raines EW. Emerging roles for ectodomain shedding in the regulation of inflammatory responses. J Leukoc Biol. 2006; 79:1105–1116. [PubMed: 16565325]
49. Nakamura H, Yoshimura K, McElvaney NG, Crystal RG. Neutrophil elastase in respiratory epithelial lining fluid of individuals with cystic fibrosis induces interleukin-8 gene expression in a human bronchial epithelial cell line. J Clin Invest. 1992; 89:1478–1484. [PubMed: 1569186]

50. Kuwahara I, Lillehoj EP, Lu W, Singh IS, Isohama Y, Miyata T, Kim KC. Neutrophil elastase induces IL-8 gene transcription and protein release through p38/NF-κB activation via EGFR transactivation in a lung epithelial cell line. Am J Physiol Lung Cell Mol Physiol. 2006; 291:L407–L416. [PubMed: 16632517]
51. Lappalainen U, Whitsett JA, Wert SE, Tichelaar JW, Bry K. Interleukin-1β causes pulmonary inflammation, emphysema, and airway remodeling in adult murine lung. Am J Respir Cell Mol Biol. 2005; 32:311–318. [PubMed: 15668323]
52. Couillin I, Vasseur V, Charron S, Gasse P, Tavernier M, Guillet J, Lagente V, Fick L, Jacobs M, Coelho FR, Moser R, Ryffel B. IL-1R1/MyD88 signaling is critical for elastase-induced lung inflammation and emphysema. J Immunol. 2009; 183:8195–8202. [PubMed: 20007584]
53. Nakayama Y, Odagaki Y, Fujita S, Matsuoka S, Hamanaka N, Nakai H, Toda M. Clarification of mechanism of human sputum elastase inhibition by a new inhibitor, ONO-5046, using electrospray ionization mass spectrometry. Bioorg Med Chem Lett. 2002; 12:2349–2353. [PubMed: 12161131]
54. Okumura HS, Philmus B, Portmann C, Hemscheidt TK. Homotyrosine-containing cyanopeptolins 880 and 960 and anabaenopeptins 908 and 915 from *Planktothrix agardhii* CYA 126/8. J Nat Prod. 2009; 72:172–176. [PubMed: 19115837]
55. Otwinowski Z, Minor W. Processing of X-Ray diffraction data collected in oscillation mode. Methods Enzymol. 1997; 276:307–326.
56. Vagin A, Teplyakov A. MOLREP: an automated program for molecular replacement. J Appl Crystallogr. 1997; 30:1022–1025.
57. Winn MD, Ballard CC, Cowtan KD, Dodson EJ, Emsley P, Evans PR, Keegan RM, Krissinel EB, Leslie AGW, McCoy A, McNicholas SJ, Murshudov GN, Pannu NS, Potterton EA, Powell HR, Read RJ, Vagin A, Wilson KS. Overview of the CCP4 suite and current developments. Acta Crystallogr D Biol Crystallogr. 2011; 67:235–242. [PubMed: 21460441]
58. Murshudov GN, Skubak P, Lebedev AA, Pannu NS, Steiner RA, Nicholls RA, Winn MD, Long F, Vagin AA. REFMAC5 for the refinement of macromolecular crystal structures. Acta Crystallogr D Biol Crystallogr. 2011; 67:355–367. [PubMed: 21460454]
59. Emsley P, Cowtan K. Coot: model-building tools for molecular graphics. Acta Crystallogr D Biol Crystallogr. 2004; 60:2126–2132. [PubMed: 15572765]
60. Liu Y, Salvador LA, Byeon S, Ying Y, Kwan JC, Law BK, Hong J, Luesch H. Anticolon cancer activity of largazole, a marine-derived tunable histone deacetylase inhibitor. J Pharmacol Exp Ther. 2010; 335:351–361. [PubMed: 20739454]
61. Huang DW, Sherman BT, Lempicki RA. Systematic and integrative analysis of large gene lists using DAVID Bioinformatics Resources. Nat Protoc. 2009; 4:44–57. [PubMed: 19131956]
62. Huang DW, Sherman BT, Lempicki RA. Bioinformatics enrichment tools: paths toward the comprehensive functional analysis of large gene lists. Nucleic Acids Res. 2009; 37:1–13. [PubMed: 19033363]

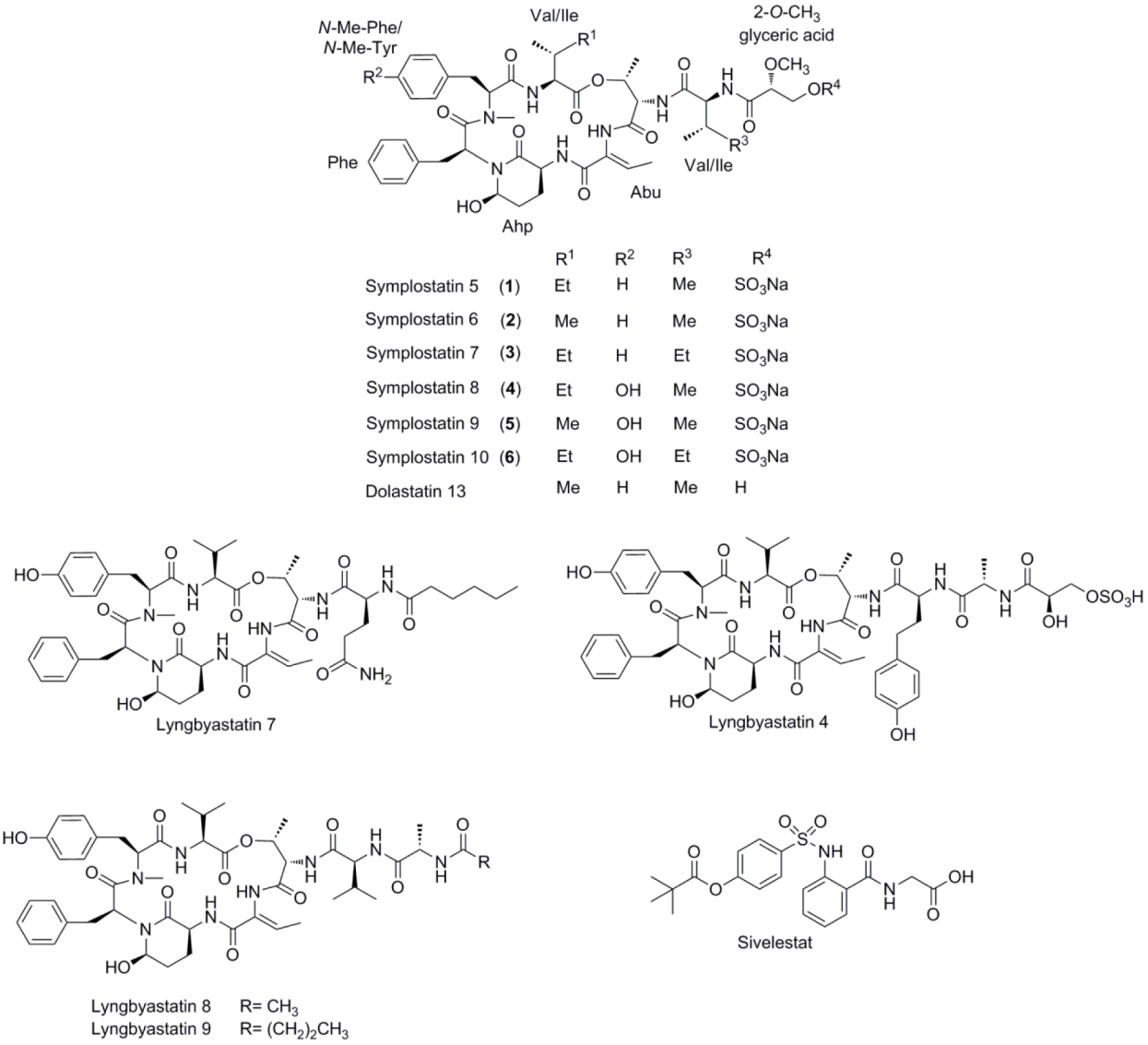

Figure 1.
Elastase inhibitors from marine cyanobacteria and the clinically approved human neutrophil elastase inhibitor sivelestat.

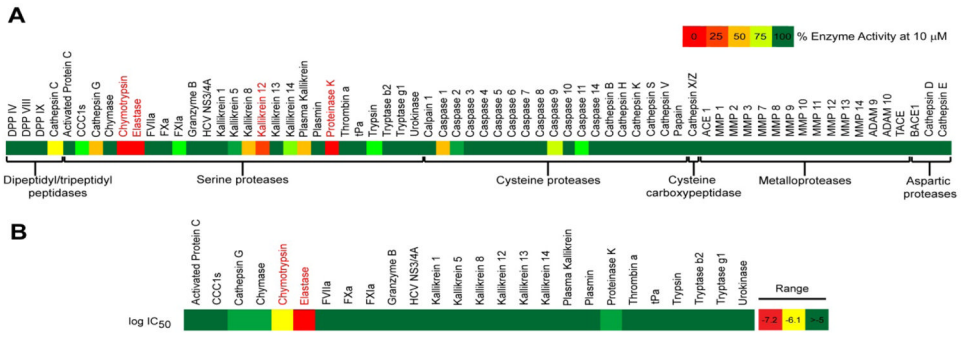

Figure 2.

Selectivity profile of Abu-containing cyclic depsipeptides from marine cyanobacteria. (**A**) Screening of lyngbyastatin 7 (10 μM) against a panel of 68 proteases. (**B**) Selectivity profiling for compound **1** on a panel of 26 serine proteases.

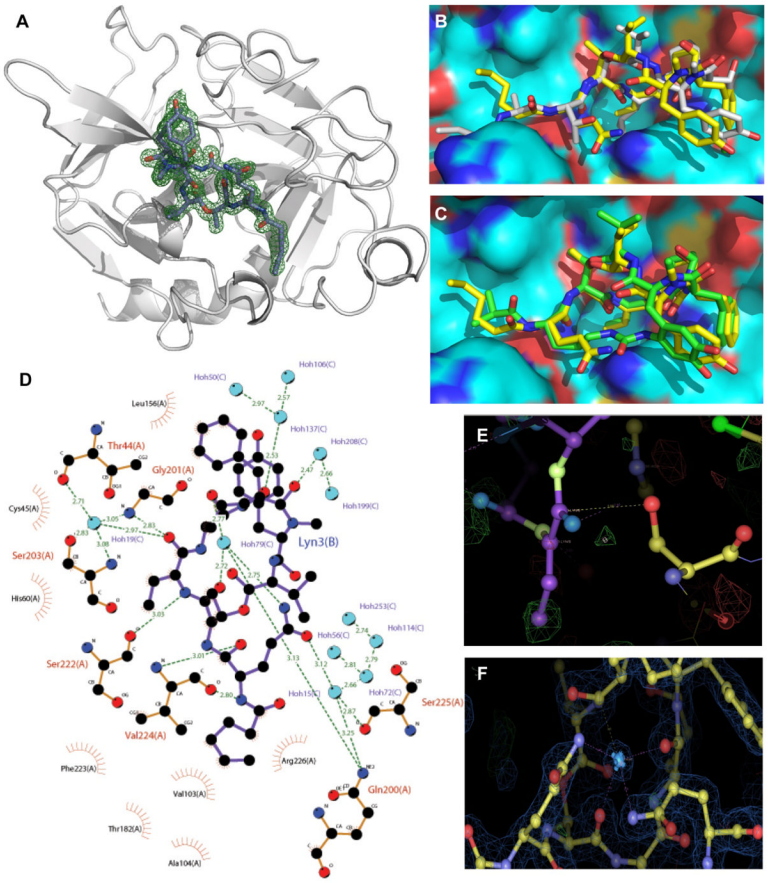

Figure 3.

Cocrystal structures of natural cyclic depsipeptide elastase inhibitors. (**A**) (F_o-F_c) plot for lyngbyastatin 7. (**B**) Comparison of lyngbyastatin 7 (yellow, PDB ID 4GVU) and scyptolin (white, PDB ID 1OKX) binding to elastase. (**C**) Comparison of lyngbyastatin 7 (yellow) and FR901277 (green, PDB ID 1QR3) binding to elastase. (**D**) Ligplot of the lyngbyastatin 7–porcine pancreatic elastase complex. The Abu moiety serves as the key residue for elastase inhibition. Chain designations are (A) elastase, (B) lyngbyastatin 7, (C) H_2O. (**E**) Proposed CH-π interaction between the catalytic Ser203 and the Abu moiety. (**F**) Network of inter- and intramolecular hydrogen bonding interaction in lyngbyastatin 7 mediated by a water molecule.

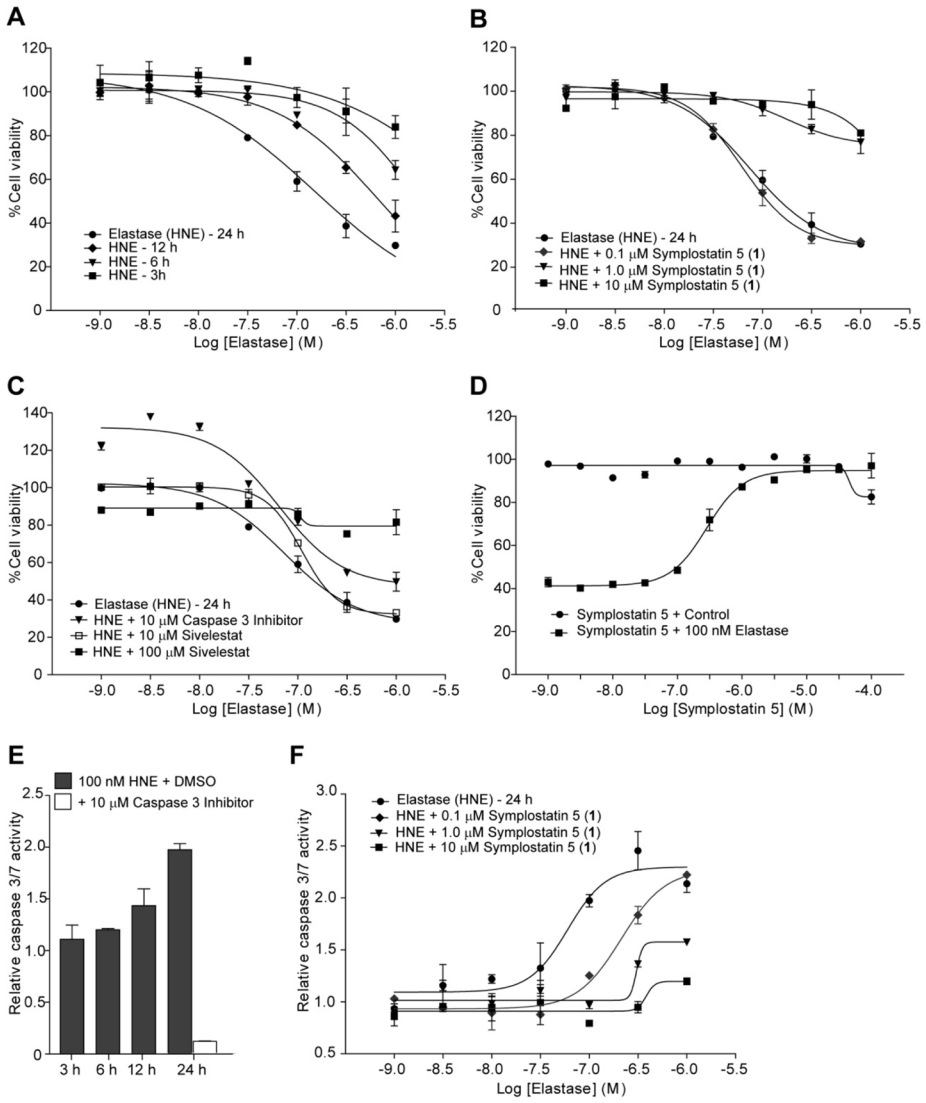

Figure 4.

Changes in cell viability and caspase activation mediated by elastase and effects of inhibitors. (**A**) Elastase displayed both time- and dose-dependent decrease in cell viability, with substantial changes at 12–24 h. (**B**) Compound **1** attenuated the antiproliferative effects of elastase. (**C**) Sivelestat and the caspase 3 inhibitor Z-D(OMe)E(OMe)VD(OMe)-FMK also partially protected against the antiproliferative effects of elastase. (**D**) Compound **1** did not show any significant antiproliferative effect on BEAS-2B cells at 24 h. (**E**) Treatment with 100 nM elastase caused a time-dependent increase in caspase activation which was abrogated by the caspase 3 inhibitor. (**F**) Incubation of BEAS-2B cells with elastase for 24 h caused a dose-dependent increase in caspase 3/7 activity. Compound **1** attenuated the potency and efficacy of elastase to activate distal caspases. Data are presented as mean ± SEM (n = 2).

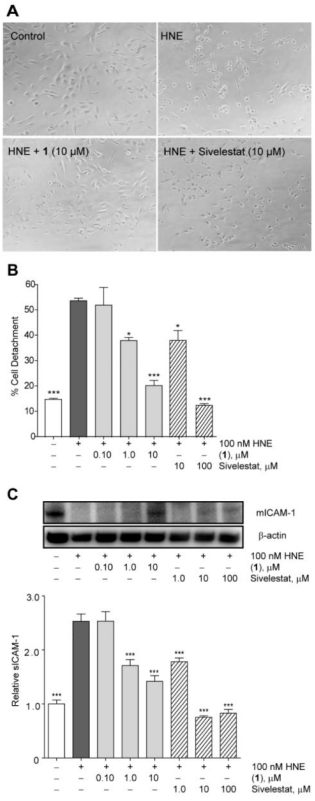

Figure 5.

Elastase acts as a sheddase and promotes cell morphology change and desquamation. (**A**) Elastase caused cell rounding after incubation for 3 h. Cotreatment with 10 μM compound **1** or sivelestat prevented this effect of elastase (10× magnification). (**B**) Significant increase in cell detachment was observed after 12 h of incubation with elastase, which was abrogated by both compound **1** and sivelestat. (**C**) Levels of mICAM-1 and sICAM-1 in whole cell lysates and culture supernatants, respectively, of elastase-treated and elastase-inhibitor co-treated cells. Data are presented as mean + SEM, * $P < 0.05$, ** $P < 0.01$, *** $P < 0.001$ compared to HNE-treated control cells using ANOVA, Dunnett's t -test (n = 3).

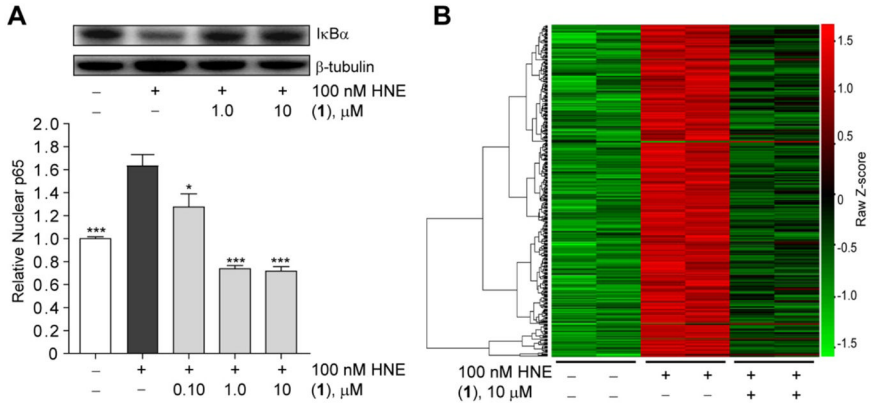

C

Probe ID	Symbol	Annotation	Fold induction[a]	% Reduction[b]
39402_at	*IL1B*	Interleukin 1B	2.91	58[c]
241786_at	*PPP3R1*	Protein phosphatase 3, regulatory subunit B	2.42	56[c]
205207_at	*IL6*	Interleukin 6	2.26	22
1569540_at	*NLK*	Nemo-like kinase	2.23	49
239409_at	*RAP1A*	RAP1A, member of RAS oncogene family	2.21	53[c]
230337_at	*SOS1*	Son of sevenless homolog 1	1.89	46[c]
210118_s_at	*IL1A*	Interleukin 1A	1.85	34
1565889_at	*TAB2*	Mitogen-activated kinase kinase 7 interacting ptotein	1.83	42
211506_s_at	*IL8*	Interleukin 8	1.53	22

[a]Relative to control, $P < 0.05$. [b] In response to inhibitor cotreatment. [c]Significant difference with inhibitor treatment, $P < 0.05$.

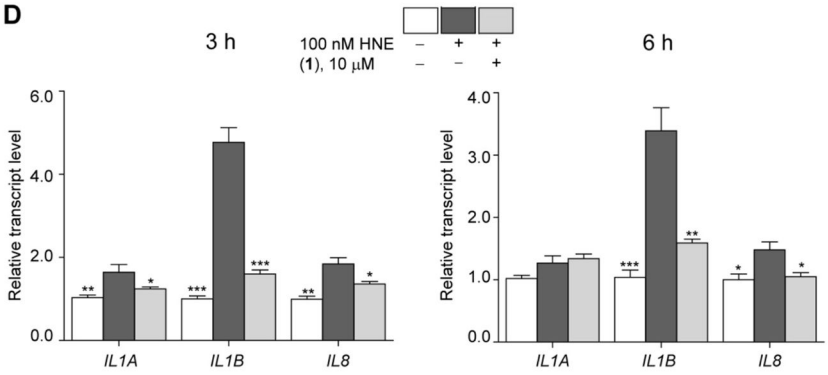

Figure 6.

Elastase caused a global change in transcript level via, in part, an NF-κB dependent pathway. (**A**) Compound **1** dose-dependently inhibited elastase-induced IκB degradation and p65 nuclear translocation at 3 h of cotreatment. (**B**) Heatmap of differentially regulated transcripts by elastase with or without compound (1) cotreatment. Global transcriptome profiling (Affymetrix GeneChip Human Genome U133 plus 2.0 arrays) was carried out using duplicate biological samples. (**C**) Relevant genes involved in NOD- and MAPK-signaling pathways that were significantly modulated by elastase (Fold change > 1.5, $P < 0.05$). (**D**) Validation of the microarray analysis using RT-qPCR. Data are presented as mean + SEM for **A** and mean + SD for **D**, * $P < 0.05$, ** $P < 0.01$, *** $P < 0.001$ compared to HNE-treated control cells using ANOVA, Dunnett's t -test (n = 3).

Table 1

NMR Data of Symplostatin 5 (**1**) in DMSO-d_6.

unit	C/H no	δ_C[a]	δ_H (J in Hz)[b]	COSY[b]	HMBC[b]
Ile	1	170.0,C			
	2	54.0, CH	4.89, br	NH	1
	3	37.5, CH	1.86, m	H_3-6	
	4a	25.8, CH_2	1.30, m	H-4b, H_3-5	2, 3
	4b		1.11, m	H-4a, H_3-5	2, 3
	5	11.2, CH_3	0.92, t (7.2)	H-4a, H-4b	3
	6	14.1, CH_3	0.71, d (7.0)	H-3	2, 3
	NH		7.40, br	H-2	
N-Me-Phe	1	172.7, C			
	2	60.2, CH	5.00, br	H-3a, H-3b	1
	3a	33.4, CH_2	3.23, brd (13.5)	H-2, H-3b	4,5/9
	3b		2.84, m	H-2, H-3a	5/9
	4	137.9, C			
	5/9	129.4, CH	7.23, d (7.5)	H-6	
	6/8	128.4, CH	7.39, m	H-5, H-7	4
	7	126.5, CH	7.30, m	H-6	
	OH				
	N-Me	30.1, CH_3	2.77, s		2, 1 (Phe)
Phe	1	170.3, C			
	2	49.6, CH	4.70, dd (11.4,4.7)	H-3a, H-3b	1, 2 (Ahp)
	3a	34.8, CH_2	2.84, dd (−14.7,11.4)	H-2, H-3b	4
	3b		1.68, m	H-2, H-3a	4
	4	136.5, C			
	5/9	129.2, CH	6.77, d (7.5)	H-6	7
	6	127.6, CH	7.18, m	H-5, H-7	4
	7	126.1, CH	7.15, m	H-6	
Ahp	2	168.7, C			
	3	47.8, CH	3.75, m	H-4a, H-4b, NH	2

unit	C/H no	δ_C[a]	δ_H (*J* in Hz)[b]	COSY[b]	HMBC[b]
	4a	21.7, CH_2	2.38, m	H-3, H-4b, H-5a	
	4b		1.56, m	H-3, H-4a	
	5a	29.0, CH_2	1.68, m	H-4a, H-5b, H-6	
	5b		1.50, m	H-5a, H-6	
	6	73.4, CH	5.03, br s	H-5a, H-5b, OH	2
	OH		6.05, s	H-6	
	NH		7.34, br	H-3	
Abu	1	162.9, C			
	2	130.0, C			
	3	131.7, CH	6.50, q (7.2)	H_3-4	1, 4
	4	12.8, CH_3	1.47, d (7.2)	H-3	1, 2
	NH		9.24, br s		
Thr	1	*c*			
	2	55.1, CH	4.67, br	NH	
	3	71.5, CH	5.52, br s	H_3-4	
	4	17.5, CH_3	1.22, d (6.5)	H-3	2
	NH		8.18, br s	H-2	
Val	1	172.2, C			
	2	56.4, CH	4.47, t (7.2)	NH	1
	3	30.7, CH	2.09, m	H_3-4, H_3-5	
	4	18.9, CH_3	0.88, d (6.7)	H-3	1
	5	17.5, CH_3	0.83, d (6.7)	H-3	1
	NH		7.71, br s	H-2	
2-*O*-CH_3 Glyceric Acid	1	168.9, C			
	2	79.9, CH	3.98, dd (7.4,3.4)	H-3a, H-3b	
	3a	66.1, CH2	3.90, dd (−10.8,3.4)	H-2, H-3b	
	3b		3.73, m	H-2, H-3a	
	OCH_3	57.1, CH_3	3.33[d]		2

[a] Deduced from HSQC and HMBC, 600 MHz.

[b] 600 MHz.

[c] No correlation observed from HMBC.

[d] Overlapping with residual water.

Table 2

Antiproteolytic Activity of Abu-containing Cyclic Depsipeptides from Marine Cyanobacteria.[a]

Compound	Porcine Pancreatic Elastase[b] IC_{50} (nM)	Human Neutrophil Elastase[c] IC_{50} (nM)	Bovine Pancreatic Chymotrypsin[d] IC_{50} (nM)	Human Pancreatic Chymotrypsin[e] IC_{50} (nM) (% Activity at 10 μM)
Symplostatin 5 (**1**)	68 ± 9.7	144 ± 2.9	322 ± 3.2	> 10000 (53.4 ± 3.2)
Symplostatin 6 (**2**)	89 ± 11	121 ± 12	503 ± 65	> 10000 (90.6 ± 7.6)
Symplostatin 7 (**3**)	77 ± 5.4	195 ± 28	515 ± 43	> 10000 (70.7 ± 3.8)
Symplostatin 8 (**4**)	43 ± 3.2	41 ± 9.0	268 ± 11	> 10000 (69.0 ± 2.0)
Symplostatin 9 (**5**)	37 ± 3.1	28 ± 5.8	324 ± 27	> 10000 (73.9 ± 1.0)
Symplostatin 10 (**6**)	44 ± 1.5	21 ± 2.9	222 ± 5.1	> 10000 (79.4 ± 3.2)
Lyngbyastatin 4	41 ± 2.0	49 ± 1.4	614 ± 6.3	> 10000 (72.2 ± 3.3)
Lyngbyastatin 7	30 ± 6.8	23 ± 1.1	314 ± 37	−2000
Sivelestat	2810 ± 95	136 ± 18	4084 ± 37	> 10000 (55.1 ± 3.3)

[a] Data are presented as mean ± SD (n = 3).

[b–e] Substrates.

[b] *N*-succinyl-Ala-Ala-Ala-*p*-nitroanilide.

[c] *N*-(methoxysuccinyl)-Ala-Ala-Pro-Val-*p*-nitroanilide.

[d] *N*-succinyl-Gly-Gly-Phe-*p*-nitroanilide.

[e] *N*-succinyl-Ala-Ala-Pro-Phe-*p*-nitroanilide.